A vertical additive-lathe printing system for the fabrication of tubular constructs using gelatin methacryloyl hydrogel

A vertical additive-lathe printing system for the fabrication of tubular constructs using gelatin methacryloyl hydrogel

Faraz Fazal[1,2], Ferry P.W. Melchels[3], Andrew McCormack[3], Andreia F. Silva[4], Anthony Callanan[5], Vasileios Koutsos[1], and Norbert Radacsi[1,*]

[1] School of Engineering, Institute for Materials and Processes, The University of Edinburgh, Robert Stevenson Road, EH9 3FB Edinburgh, United Kingdom

[2] Department of Mechanical Engineering, University of Engineering and Technology, Lahore, (New Campus) Pakistan

[3] School of Engineering and Physical Sciences, Institute of Biological Chemistry, Biophysics and Bioengineering, Heriot-Watt University, EH14 4AS Edinburgh, United Kingdom

[4] Edinburgh Complex Fluids Partnership (ECFP), SUPA and School of Physics & Astronomy, The University of Edinburgh, Peter Guthrie Tait Road, EH9 3FD Edinburgh, United Kingdom

[5] School of Engineering, Institute for Bioengineering, The University of Edinburgh, The King's Buildings, EH9 3JL Edinburgh, United Kingdom

[*] Corresponding author email address: n.radacsi@ed.ac.uk

Abstract:

Reproducing both the mechanical and biological performance of native blood vessels remains an ongoing challenge in vascular tissue engineering. Additive-lathe printing offers an attractive method of fabricating long tubular constructs as a potential vascular graft for the treatment of cardiovascular diseases. Printing hydrogels onto rotating horizontal mandrels often leads to sagging, resulting in poor and variable mechanical properties. In this study, an additive-lathe printing system with a vertical mandrel to fabricate tubular constructs is presented. Various concentrations of gelatin methacryloyl (gelMA) hydrogel were used to print grafts on the rotating mandrel in a helical pattern. The printing parameters were selected to achieve the bonding of consecutive gelMA filaments to improve the quality of the printed graft. The hydrogel filaments were fused properly under the action of gravity on the vertical mandrel. Thus, the vertical additive-lathe printing system was used to print uniform wall thickness grafts, eliminating the hydrogel sagging problem. Tensile testing performed in both circumferential and longitudinal direction revealed that the anisotropic properties of printed gelMA constructs were similar to those observed in the native blood vessels. In addition, no leakage was detected through the walls of the gelMA grafts during burst pressure measurement. Therefore, the current printing setup could be utilized to print vascular grafts for the treatment of cardiovascular diseases.

Keywords

Additive-lathe, extrusion-based printing, tubular constructs, gelatin methacryloyl, burst pressure, anisotropic index

1 Introduction

Cardiovascular diseases, such as coronary heart disease, aortic disease, and peripheral artery disease are the primary causes of death globally [1]. The annual number of deaths due to cardiovascular diseases are predicted to reach 23 million by 2030 [2]. Bypass surgeries are performed to treat these cardiovascular diseases, in which a vascular conduit is used to bypass the blocked or damaged arteries

[3]. The use of autologous grafts, such as a saphenous vein or radial artery, remains the gold standard [4]. However, 50% of the patients lack a suitable and good quality vessel that can be used in bypass surgeries [5]. Moreover, the venous grafts show limited patency and failure rates of 50% are observed at ten years [6]. Grafts made from synthetic materials, such as Dacron, perform well when they are used for the replacement of large conduits (>6 mm) [7]. However, for small diameter vessels, these synthetic grafts fail due to intimal hyperplasia, infection, and thrombosis [8].

Tissue engineering techniques provide an alternative approach to fabricate vascular grafts [9]. Over the last two decades, several tissue engineering approaches have been developed such as molding methods [10–12], scaffold-based techniques [13–15], decellularization-based processing [16,17], and cell-sheet engineering [18,19]. Although these methods are useful for the development of a tubular vascular construct, there are several limitations associated with these techniques. Molding methods require several molds for different desired dimensions and are unable to fabricate vascular grafts with a layered structure to mimic the tunica intima, tunica media, and tunica externa, as found in the natural blood vessels [20]. The scaffold-based techniques have a long processing time and poor micro-architectural control [21]. Decellularization-based processing generally involves a high cost and can result in immune rejection, whereas cell-sheet engineering requires the use of many cell sheets which are cultured for a long time to get a vascular graft [17,22].

3D bioprinting is an emerging technology that has already attracted great attention due to its potential in the field of regenerative medicine [23]. Extrusion bioprinting [24–28], ink-jet bioprinting [29–33], laser-based bioprinting method [34,35], and stereolithography [36–38] are common modalities which have been utilized for vascular tissue engineering applications [39]. Extrusion-based bioprinting is the most widely used method [40]. In extrusion bioprinting, the printing can be done using bioinks with a wide range of viscosities, from 0.03 to 6 x 10^4 Pa·s [41]. Other advantages of the extrusion printing process over other printing methods include low setup cost, good mechanical properties of printed structures, and the capability to utilize multi-material printing heads [42–44]. In a direct extrusion bioprinting method, bioink is extruded from the nozzle to build a tubular construct in a layer-by-layer fashion [45]. To maintain the shape fidelity of a hollow-3D structure, the bioink should have sufficient mechanical strength [46]. As one way to address this challenge, a layer-by-layer UV-assisted extrusion bioprinting strategy was developed, in which the UV crosslinking was performed after printing a few layers of bioink. This resulted in a high aspect ratio of tubular constructs [47]. In another study, a bi-layered vascular construct was printed using a similar technique, in which cross-linking was done after printing every four layers of gelMA-based bioink [48]. In both of these studies, a repeated cross-linking strategy was utilized to increase the overall height of the printed construct but the maximum height achieved was in the range of 20 mm. However, functional testing including leakage and burst pressure testing were not performed in any of these studies.

To print longer vascular constructs, mandrel-based printing systems have been employed [49]. These systems are also known as additive-lathe printing systems [50]. In these setups, the hydrogel is printed around a rotating mandrel. After cross-linking, the tubular construct is removed from the rod [51,52]. In recent studies, gelatin-based hydrogels were used to print vascular grafts around a rotating mandrel [20,53]. In all the related works, a horizontal mandrel was used to print a tubular construct, which resulted in a sag on the bottom side of the printed graft due to gravity. This problem tends to get worse for hydrogels with low viscosity, e.g. as a result of low polymer concentration. A huge variation in the mechanical properties of grafts was observed due to the non-uniform wall thickness of the graft [20]. Also, many studies demonstrating printing of blood vessels using hydrogels (either with or without mandrel) do not report on burst pressure strength.

Here, we address this issue by presenting an additive-lathe printing system in which a vertical rather than horizontal mandrel was used for the fabrication of tubular constructs. The main objective of this study is to use the newly developed printing system to fabricate and test tubular constructs using gelatin-methacryloyl (gelMA) hydrogel which has been widely used in the field of regenerative medicine due to its good biological and physical characteristics [54]. We hypothesized that the gelMA filaments would fuse with each other on the vertical mandrel under the action of gravity, thus eliminating the sagging problem observed in grafts printed on the horizontal mandrel. This would result in the printing of good quality constructs with uniform wall thickness.

2 Materials and methods

2.1 Synthesis of gelMA

Gelatin-methacryloyl (gelMA) was prepared by reaction of type A gelatin (300 Bloom, Sigma Aldrich) derived from porcine skin tissue with methacrylic anhydride (Sigma Aldrich) for 1 hour at 50 °C. The experimental procedure was based on a previously described protocol developed by Van den Bulcke *et al.* [55]. Briefly, methacrylic anhydride was added dropwise to a 10% (w/v) solution of gelatin in phosphate-buffered saline (Fisher BioReagents), under constant stirring. Methacrylic anhydride was added at a ratio of 0.02 g per 1 g of gelatin. Before the addition of anhydride, the pH of the gelatin solution was adjusted to pH 8, with the addition of 5M NaOH solution. Following the reaction, centrifugation, decanting, and dialysis (cellulose membrane, cut-off 12 kDa) against distilled water were performed to remove methacrylic acid and anhydride. The gelMA macromonomer solution was pH-neutralised and then lyophilised and stored at -20 °C until use.

2.2 ^{1}H-NMR

The degree of functionalisation (*DoF*) of gelMA macromonomer was quantified using proton-nuclear magnetic resonance spectroscopy (^{1}H-NMR, Bruker AVIII 300MHz). Before the ^{1}H-NMR experiment, 50 mg of either the gelMA macromonomer or the corresponding gelatin sample, were dissolved in 1 mL of deuterium oxide (D_2O) at 37 °C. A sample of 0.8 mL of the gelMA or gelatin solution was used for the ^{1}H-NMR experiments. The DoF was calculated from Equation 1 below.

$$DoF = 1 - \left(\frac{lysine\ methylene\ proton\ of\ GelMA\ (2.9\ ppm)}{lysine\ methylene\ proton\ of\ gelatin\ (2.9\ ppm)}\right) \times 100\ \% \quad (1)$$

2.3 Preparation of gelMA hydrogel

GelMA hydrogel was prepared by first dissolving 0.3% (w/v) lithium phenyl-2,4,6-trimethylbenzoylphosphinate (LAP) in PBS at 60 ℃ for 10 min. The freeze-dried gelMA was weighed and added to the solution to achieve concentrations of 7.5%, 10%, and 12% (w/v) gelMA hydrogel. The solutions were stirred on the hot plate for 2 hours at 60 ℃. After stirring, the clear gelMA solutions were kept in the water bath for 2 – 5 minutes at specific temperatures required for printing (Table 1).

2.4 The configuration of the vertical additive-lathe 3D printing system

A vertical additive-lathe 3D printing system was developed as described previously [56]. Briefly, this printing system consists of a vertical mandrel mounted on a NEMA14 stepper motor and a printing head assembly as shown in the Fig. 1a. The printing head assembly is tilted at an angle of 15° with respect to the vertical axis to facilitate the printing process. The printer is controlled by an Arduino mega 2560 and a Ramps 1.4 controller board. To print the tubular construct, the vertical mandrel was rotated at 20 rev min^{-1}. A pre-warmed gelMA hydrogel is loaded in a 1 mL syringe with a Luer lock. The environment temperature was recorded as 19 – 21 ℃ during all printing runs. Typical printing time to print one construct ranged from 2 to 5 minutes. The printing head moved in the z-axis direction while dispensing the gelMA hydrogel onto the rotating mandrel in a helical pattern. The hydrogel was

extruded from an 18 G tapered tip (0.838 mm ID). The hydrogel extrusion flow rates ranged from 0.15 mL min^{-1} to 0.30 mL min^{-1}. After printing, the gelMA constructs were cross-linked using 10W 1P66 lamp (405 nm, 0.44 mW cm^{-2} intensity at 2 cm distance) for 10 minutes.

2.5 Rheological testing

All the rheological testing was done on a Discovery Hybrid Rheometer 2.0 (TA Instruments, United States). A 40 mm sandblasted parallel plate and a measuring gap of 300 µm was used for all the test runs. A solvent trap was used in all measurements to minimise evaporation. For all the gelMA concentrations, an oscillatory strain sweep was performed to determine the linear viscoelastic (LVE) region. The storage and loss modulus were determined using an angular frequency of 10 rad sec^{-1} and for a temperature range of 5 ℃ to 40 ℃. Next, the viscosity of the gelMA hydrogel was measured using a temperature ramp at a constant shear rate of 10 s^{-1} from 40 ℃ to 5 ℃ at a cooling rate of 3 ℃/min.

2.6 Mechanical testing

The tensile testing of 7.5%, 10%, and 12% gelMA tubular constructs, was done in the circumferential and longitudinal directions on Instron 3367 universal testing machine (Instron, High Wycombe, UK) using 50 N Load cell. All the gelMA samples were tested in a fully hydrated state. For circumferential tensile testing, the ringlet samples (inner diameter of 4 mm, the thickness of 0.6 mm, and length of 8 mm) were cut using a scalpel. A set of specially designed clamps with two steel pins (1 mm diameter) were used to stretch the ringlet samples in the circumferential direction at a constant crosshead speed of 11 mm min^{-1}. Using the sample dimensions, the recorded load and displacement data was converted to circumferential stress and strain. The corresponding Young's modulus (E_c) was calculated from the slope of a linear region of stress-strain curves ranging from 0 to 10% strain. The circumferential tensile strength of all the samples was also determined from the stress-strain curve as the maximum value of stress until failure. The burst pressure was estimated using the following formula (Barlow's equation) [39,57],

$$P_{Burst} = 2t \times CS/OD \quad (2)$$

Where t is the wall thickness of the specimen, OD is the outer diameter, and CS is the circumferential tensile strength.

For longitudinal tensile testing, the tubular specimen with an inner diameter of 4 mm, a thickness of 0.8 mm, and a length of 12 mm were stretched at a crosshead speed of 11 mm min^{-1} until failure. Rough sandpaper was glued to the clamps to avoid slippage during tensile testing. The corresponding Young's modulus (E_z) was determined at 10% strain. The anisotropic index was calculated using the following formula,

$$I = E_c/E_z \quad (3)$$

Where E_c and E_z are the Young's modulus values of the specimen when stretched in the circumferential and longitudinal direction, respectively.

All measurements were performed in triplicate.

2.7 Burst pressure testing

The burst pressure testing was performed at room temperature on Instron 3367 universal testing machine (Instron, High Wycombe, UK) [58]. The gelMA grafts were mounted on 8 G blunt stainless steel needle tips (AD8SS-1/2, 4.03 mm OD) from both the ends, with one tip sealed to avoid any

leakage during testing. The other tip was attached to a water-filled 10 mL glass syringe, which was mounted on the rig made from polymethyl methacrylate parts as shown in Fig. S2. The joint between the graft and needle was made leak-proof using cable ties and yarn knots. All the tests were performed with a constant crosshead speed of 25 mm min^{-1}, which is equivalent to 4.2 mL min^{-1}. The net force is calculated by subtracting the friction force from the measured force. The friction force is measured by recording the force on the water-filled syringe plunger without having any graft. The burst pressure is calculated by dividing the maximum net force by the syringe plunger surface area (166.75 mm^2).

2.8 Statistics

All the results are presented as mean ± standard deviation. The wall thickness results were analysed using two way ANOVA. A $p < 0.05$ was considered as statistically significant.

3 Results

3.1 GelMA synthesis confirmation and degree of functionalization

The modification of gelatin by reaction with methacrylic anhydride was confirmed using ^{1}H-NMR spectroscopy. The spectra, including proton identification, is shown in Fig. S1. The amine group conversion to methacrylamide was determined from the ratio of integrals of the peak around 2.9 ppm corresponding to lysine and was found to be 41 ± 2%. Additional peaks were observed around 5.5 ppm representing the acrylic protons on the methacrylamide group. The residual signals of the gelMA spectrum showed similar chemical shifts and intensities to those of the gelatin, indicating the primary structure of the gelatin molecule was unaffected by the functionalisation procedure.

3.2 Fabrication of tubular constructs

A vertical additive lathe 3D printing system was made to print a tubular graft (Fig. 1a). A stainless steel rod with an outer diameter of 4 mm was chosen. The gelMA grafts printed on this mandrel fall in the category of small-diameter vascular grafts, as the inner diameter of the printed construct is less than 6 mm. To print a smooth construct on the rotating mandrel, the following formula was used to achieve the synchronization between three linear velocities (V_z, V_e, and V_r) during printing, as shown in the Fig. 1b,

$$V_e = V_r + V_z \qquad (4)$$

Where V_e is the linear velocity of hydrogel extrusion from nozzle tip, V_r is the linear velocity of the mandrel, and V_z is the linear velocity of nozzle travelling in the z-axis. The nozzle velocity V_z is calculated by using the following formula,

$$V_z = P \times N \qquad (5)$$

Where P is the pitch of the hydrogel printing filament and N is the rotational speed of the mandrel. To improve the printed construct quality, the vertical velocity of the nozzle is selected as 0.75 times the linear velocity of the nozzle ($0.75 \times P \times N$). This resulted in the overlapping of consecutive hydrogel filaments to improve the quality and subsequently the strength of the cross-linked tubular construct. The comparison between the higher, normal, and reduced vertical velocity of the nozzle in the z-axis is shown in the Fig. 1c, 1d, and 1e, respectively, whereas the actual construct printed with nozzle travel velocity as 0.75 times the V_z is shown in the Fig. 1f. After crosslinking, the printed graft was removed from the mandrel (Fig. 1g). The printing parameters used on the vertical additive lathe 3D printing setup are shown in the Table. 1. To demonstrate the versatility of this technique, a bi-layered tubular construct was printed, as shown in the Fig. 1 (h-i). The wall thickness of the first and second layer of this bi-layered construct was 0.53 ± 0.02 mm and 0.86 ± 0.04 mm, respectively. This multi-layered

printing feature of the current printing method can be utilized to mimic the layered architecture of natural blood vessels.

Table 1. Printing parameters of vertical additive lathe 3D printing setup.

Printing parameter	Value
Printing temperature of 7.5% gelMA	22 ℃
Printing temperature of 10% gelMA	27 ℃
Printing temperature of 12% gelMA	31 ℃
Mandrel temperature	19 ℃
Mandrel RPMs	20 rev min^{-1}
Extruder motor RPMs	1.014 – 2.027 rev min^{-1}
Z-axis motor RPMs	1.573 rev min^{-1}
Flow rate of gelMA hydrogel	0.15 – 0.30 mL min^{-1}
gelMA hydrogel filament pitch	0.629 mm
Printing speed	12.580 mm min^{-1}

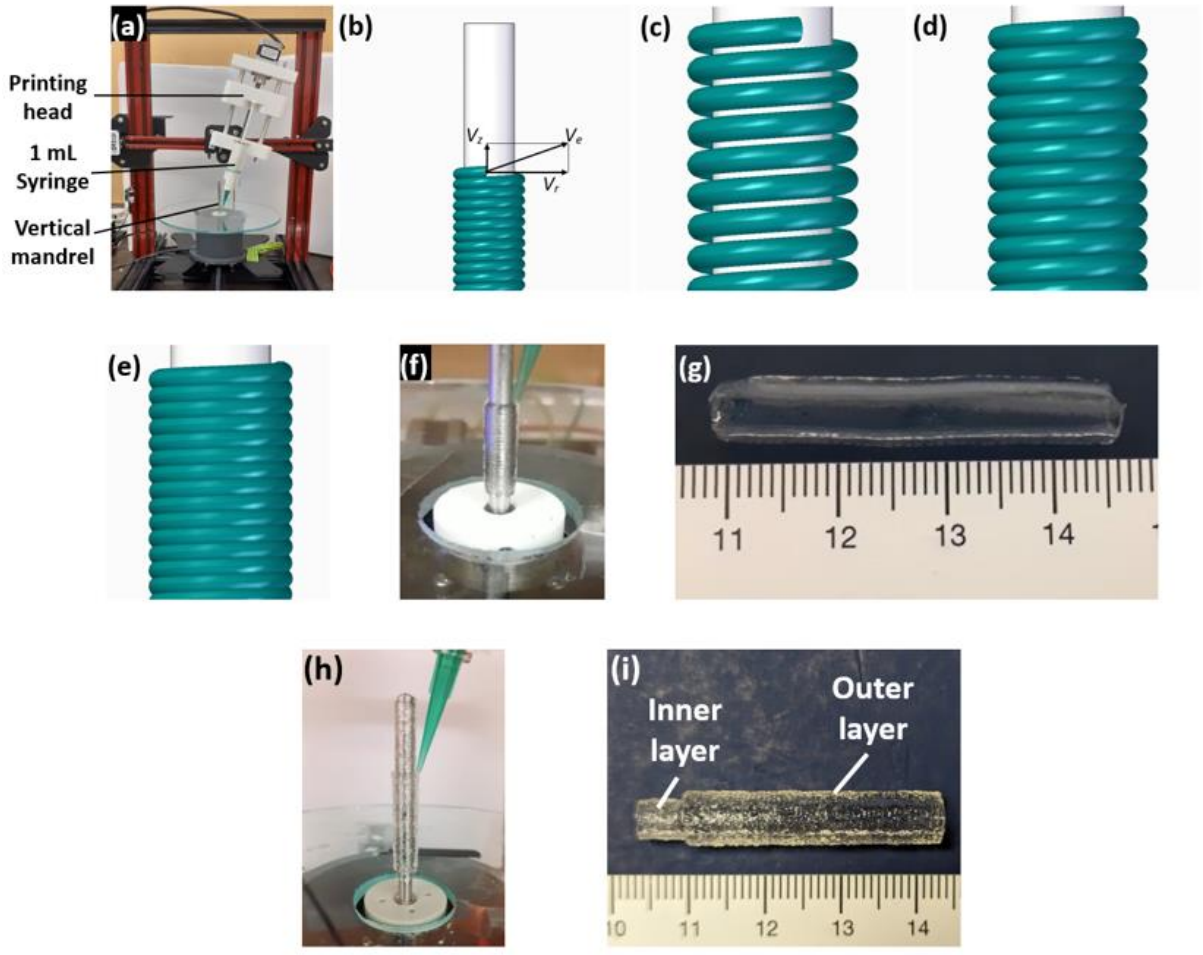

Figure 1. Vertical additive lathe 3D printing system, (a) Printing setup, (b) Velocity vector diagram to achieve synchronized printing of gelMA tubular construct, (c) Schematic diagram of hydrogel filament on the rotating mandrel printed with higher vertical velocity (equal to 1.25 times V_z), (d) Schematic diagram of hydrogel filament on the rotating mandrel printed with normal vertical velocity (equal to V_z), (e) Schematic diagram of hydrogel filament on the rotating mandrel printed with reduced vertical velocity (equal to 0.75 times V_z), (f) Actual printed gelMA construct with nozzle

z-axis velocity equal to 0.75 times V_z, (g) A full-length gelMA graft, (h) Printing of outer layer of gelMA over the inner layer to fabricate a bi-layered construct, (i) A bi-layered vascular graft removed from the mandrel.

The extruder motor RPMs were controlled to vary the hydrogel flow rate, and subsequently the wall thickness of the printed construct. The wall thickness of the printed construct could be increased by increasing the hydrogel flow rate through the nozzle, as shown in Fig. 2. The wall thickness at top, middle, and bottom cross-sections of the grafts were found to be close to each other at a given extrusion flow rate (Fig. 2b and 2c). Thus, the hydrogel adhered to the rotating mandrel properly and there was no evidence of hydrogel flowing down the mandrel during printing.

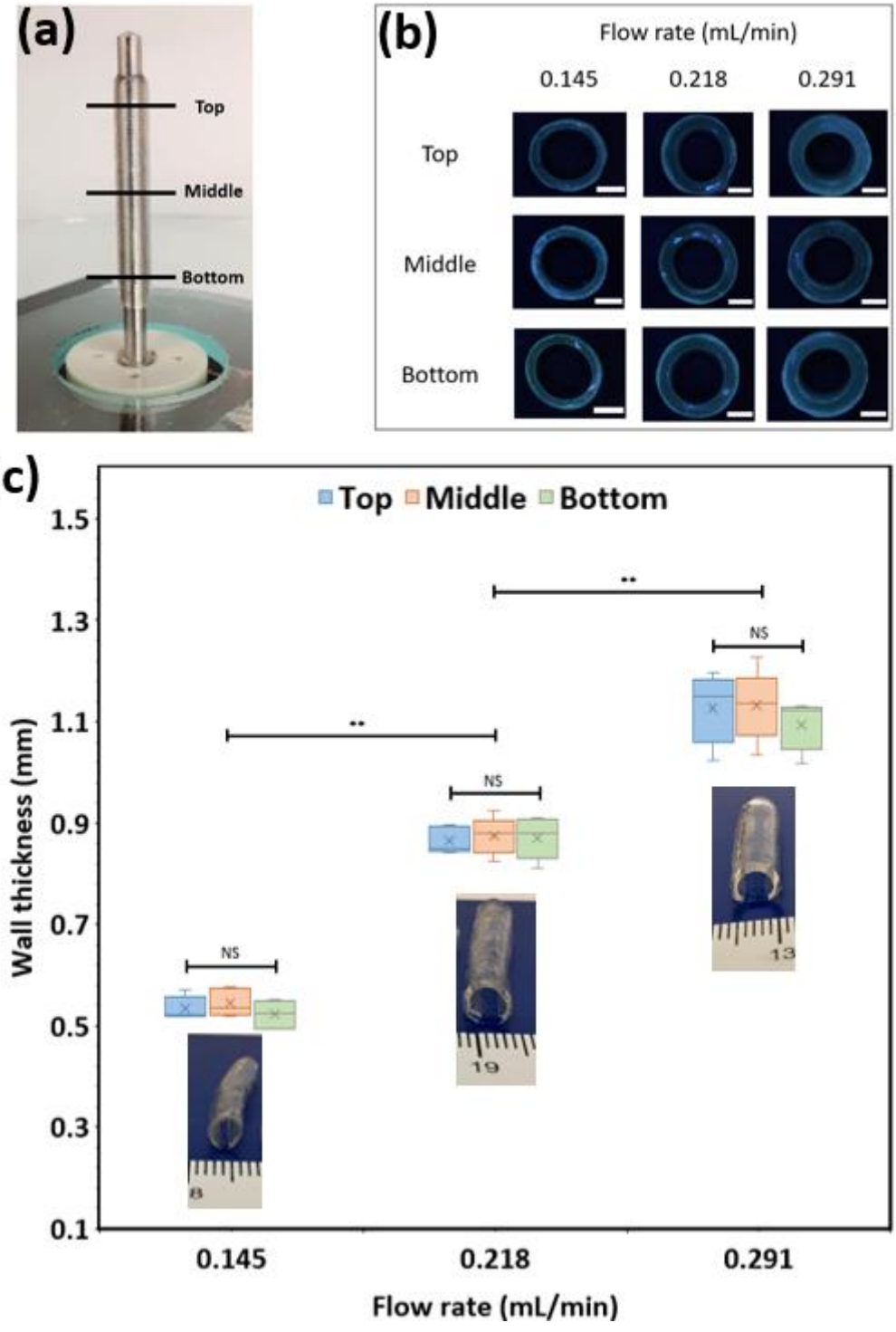

Figure 2. Wall thickness of the printed tubular construct as a function of hydrogel flow rate, (a) Top, middle, and bottom sections of the graft at which the thickness is measured, (b) Top, middle and bottom cross-sections of grafts at low, medium, and high extrusion flow rates of hydrogel (Scale bar: 2 mm), (c) Wall thickness assessment of grafts as a function of hydrogel extrusion flow rate (**, P < 0.001; NS, not significant).

3.3 Rheological testing

The rheological properties of all three gelMA concentrations (7.5%, 10%, and 12%) were evaluated. The storage and loss modulus were determined as a function of temperature, as shown in the Fig. 3a. The storage modulus (*G'*) shows the elastic component of the hydrogel, whereas the loss modulus (*G''*) measures the viscous component. At higher temperatures, the loss modulus for all three concentrations of gelMA is higher than the storage modulus. The temperature at which the storage modulus intersects the loss modulus is referred to as a sol-gel transition temperature. The sol-gel transition temperatures of 7.5%, 10%, and 12% gelMA were found to be 20.0 ± 0.2 ℃, 24.1 ± 0.2 ℃, and 25.5 ± 0.2 ℃, respectively. The printing temperatures of all hydrogels were slightly higher than the respective sol-gel temperatures, which suggests that printing was done with the polymer showing liquid-like behaviour closer to the sol-gel temperature. At these temperatures, the hydrogel filaments were able to stick to the rotating vertical mandrel (kept at room temperature) and good quality grafts were printed as shown in the Fig. 1g. The viscosity estimation was also done using a temperature ramp ranging from 40 ℃ to 5 ℃ for all the concentrations of gelMA hydrogels (Fig. 3b). According to the printing temperatures (as shown in the table. 1), the viscosity of 7.5%, 10%, and 12% gelMA was found to be 31.3 ± 2.5 mPa·s, 30.1 ± 18.0 mPa·s, and 36.5 ± 8.1 mPa·s, which reveals that the viscosity values were similar for all gelMA concentrations during the printing process.

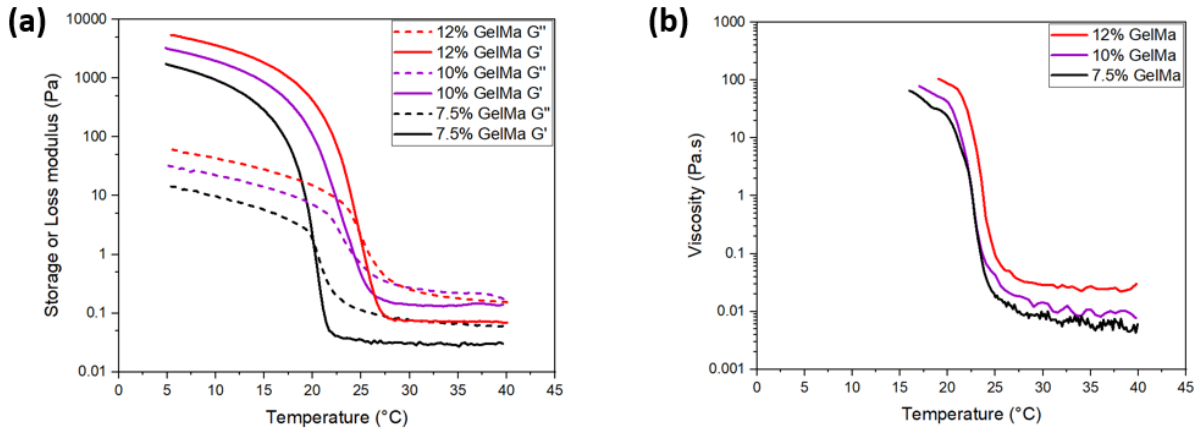

Figure 3. Rheological properties of gelMA hydrogels, (a) Storage (*G'*) and loss modulus (*G''*) as a function of temperature at an angular frequency of 10 rad sec^{-1}, (b) Viscosity as a function of temperature at a shear rate of 10 s^{-1} (cooling rate: 3 ℃/min).

3.4 Mechanical characterization

Both the circumferential and longitudinal tensile testing were performed on the gelMA tubular grafts. The Young's modulus and ultimate tensile strength followed a similar trend resulting in higher strength and modulus values with the increase in the gelMA concentration when stretched in the circumferential and longitudinal direction, as shown in the Fig. 4a and 4b. The circumferential tensile strength values were found to be 13 ± 6 kPa, 36 ± 4 kPa, and 101 ± 11 kPa for 7.5%, 10%, and 12% gelMA grafts, respectively. The mean burst pressure values were estimated using Barlow's equation and were calculated as 22.42 mmHg, 62.88 mmHg, and 174.23 mmHg for 7.5%, 10%, and 12% gelMA tubular constructs, respectively. The strain at break in the circumferential direction was higher than

that in the longitudinal direction. This suggests that the printed tubular construct can withstand sudden changes in loading without any premature failure. For all printed grafts, gelMA with a low degree of functionalization was used, which is the reason for getting higher strain at break values. The circumferential elastic modulus (E_c) of the gelMA grafts was found to be lower than the axial elastic modulus (E_z) for 10% and 12% gelMA constructs, whereas similar *Ec* and *Ez* values were observed for 7.5% gelMA grafts (Fig. 4c). Using these modulus values, the anisotropic index (*I*) is calculated for all the grafts, as shown in Fig. 4d. The anisotropic index value equal to unity shows that the grafts are equally stiff in both axial and circumferential directions, thus representing isotropic material. The constructs printed using 10% and 12% gelMA showed that the *I* value is less than one. The longitudinal stress-strain curves of the printed grafts suggest that the gelMA filaments were attached properly to each other during the helical printing process and a smooth tubular construct was fabricated.

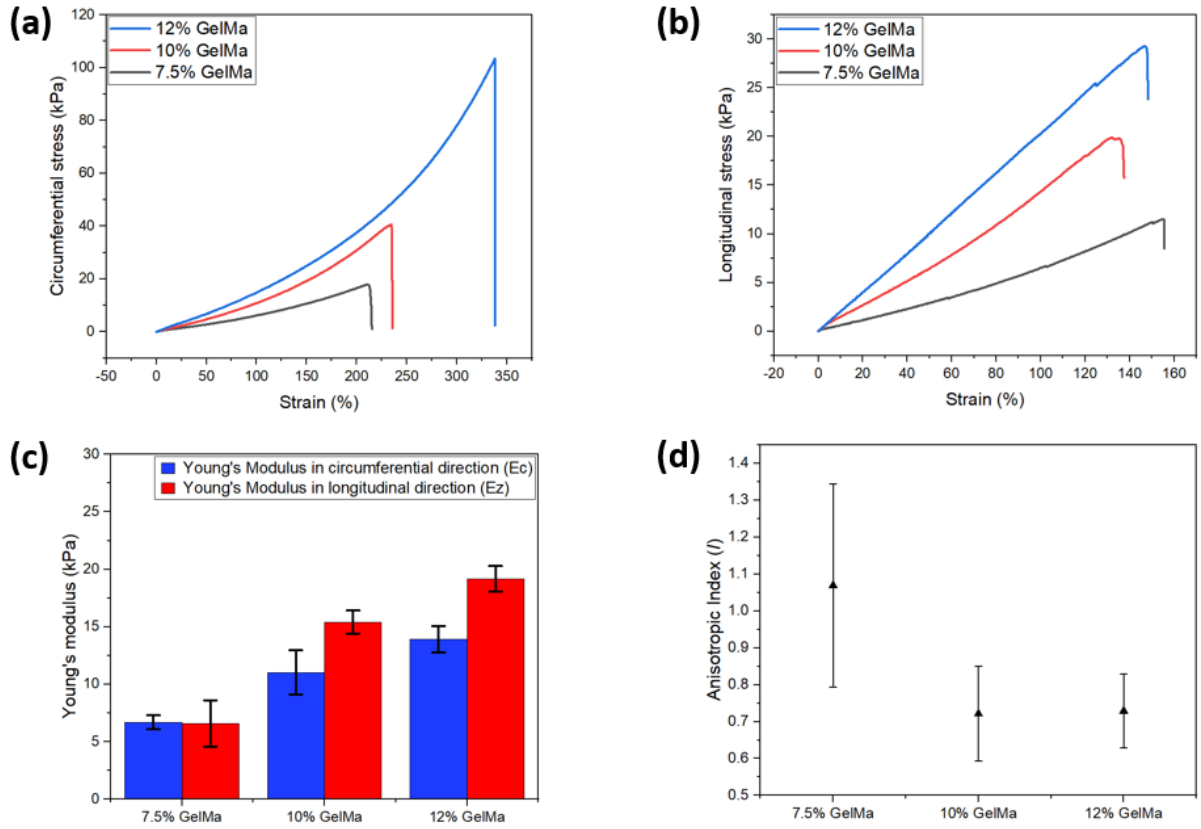

Figure 4. Mechanical testing results of gelMA tubular constructs, (a) Circumferential stress-strain curves for 7.5%, 10%, and 12% gelMA constructs, (b) Longitudinal stress-strain curves for 7.5%, 10%, and 12% gelMA constructs, (c) Young's modulus of gelMA constructs in circumferential and longitudinal directions, (d) Anisotropic index values of gelMA constructs.

3.5 Burst pressure measurement

The burst pressure was measured on Instron mechanical testing machine using a rig. Mostly in literature, the burst pressure of 3D-printed grafts made from horizontal additive-lathe technology is not measured directly and is usually estimated from Barlow's equation using tensile testing data [20]. The possible reason could be poor and inconsistent properties due to the sagging problem observed in the grafts printed around a horizontal mandrel. Using the current method of the vertical additive-lathe printing process, the burst pressure measurement results revealed better graft quality with no leakage, as shown in Fig. 5a and Fig. S3. These results showed that gravity played an important role in fusing the hydrogel filaments during the helical printing process. Also, the failure line was usually

observed in the longitudinal direction of the graft, as shown in Figure S3 (e-f), which suggests that failure occurred due to the hoop stresses developed as a result of the applied pressure during burst pressure testing. As expected, the burst pressure of the grafts was directly related to the gelMA concentration (Fig. 5b). The estimated burst pressure values calculated from Barlow's equation were higher than the measured ones. This is possibly due to the fact that the change in the cross-sectional area is neglected in Barlow's equation, whereas the direct measurement of burst pressure involved reduction in the wall thickness of grafts during test. Also, even a pin-hole development is regarded as a failure point in burst pressure testing, whereas maximum circumferential stress at complete rupture is considered for the estimation of burst pressure.

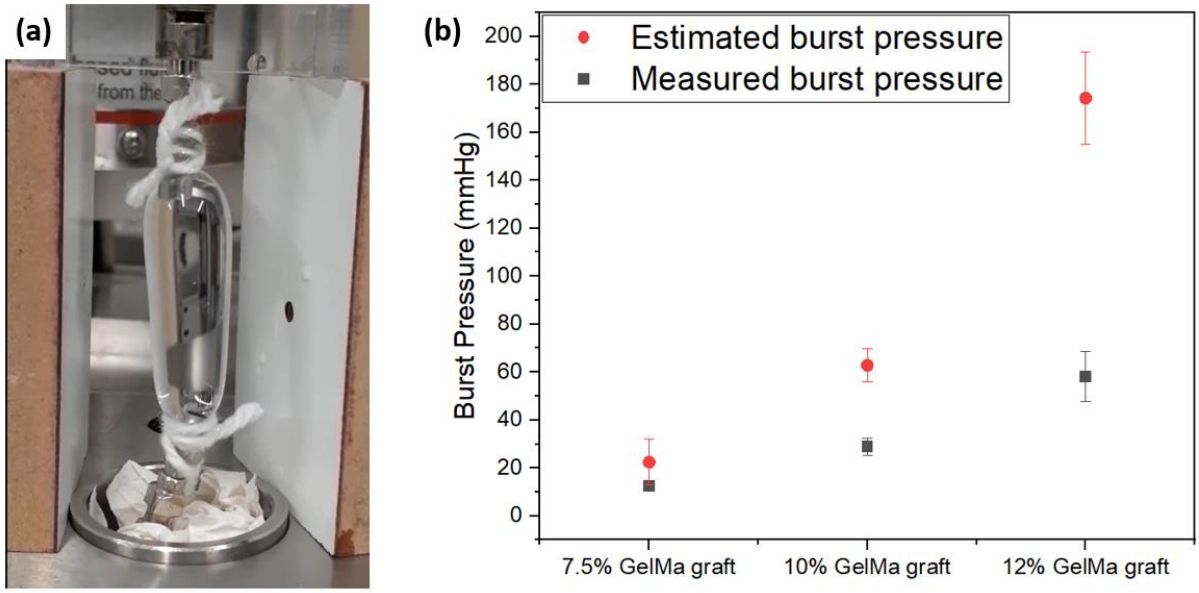

Figure 5. Burst pressure testing of gelMA grafts, (a) 12% gelMA graft during burst pressure testing, (b) Estimated and measured burst pressure values for 7.5%, 10%, and 12% gelMA grafts.

4 Discussion

We demonstrated that the current printing system with vertical mandrel is very useful for the fabrication of long and good quality grafts. The sagging problem observed in the case of the horizontal mandrel-printing system could be eliminated by using a vertical additive-lathe printing setup. In addition, the setup could be easily scaled-up by simply using a longer mandrel. The longer grafts are required for the surgeries to treat peripheral artery disease. In this work, another printing strategy was implemented in which the actual velocity of the printing head in the z-axis direction was set as 0.75 times the calculated upward linear velocity of the nozzle. This resulted in the overlapping of the two consecutive gelMA filaments during printing on the rotating rod as shown in Fig. 1 (e-f). After cross-linking, the tubular construct could be removed from the mandrel. This overlapping of hydrogel filaments is difficult to implement during printing on the horizontal mandrel as it will cause accumulation of the hydrogel, thus contributing to the sagging problem [52].

The hydrogel printing temperature is another important parameter, which is required to be controlled for printing good quality grafts. If the hydrogel temperature is too low, premature gelation will occur and the graft surface will become irregular. Whereas, the hydrogel will flow off the mandrel under the action of gravity if the hydrogel temperature is too high during printing. The sol-gel transition in gelatins is not a sharp but a broad transition, with intermediate states of partial physical crosslinking resulting in intermediate rheological properties that can be exploited for printing [59]. In this study, the pre-warmed hydrogel temperatures selected for different concentrations of gelMA were slightly

higher than their respective gelation temperatures observed in rheometry. As the hydrogel was extruded from the nozzle, it adhered to the rotating mandrel, which was kept at room temperature (19 ℃).

GelMA hydrogel was selected for printing grafts as it closely resembles the native extra-cellular matrix and it contains arginine-glycine-aspartic acid (RGD) sequences to promote cell attachment [60]. Therefore, cell-laden gelMA hydrogel could be used to print vascular grafts on the vertical additive-lathe printing setup. In many studies, additives were used with gelMA hydrogel to improve the printability of bioinks, such as gellan gum, gelatin, glycerol, and hyaluronic acid [20,47,48,61]. Whereas in this work, no additive is used in the hydrogel to improve its viscosity for printing. Therefore, it is demonstrated that gelMA hydrogel could be printed on a vertical mandrel just by controlling the temperature of the pre-warmed hydrogel.

The mechanical characterization results showed that the circumferential tensile strength of grafts was higher than the longitudinal strength. Also, a nonlinear stress-strain response was observed when the gelMA grafts were strained in the circumferential direction. The calculated values of the anisotropic index revealed that Young's modulus in the longitudinal direction is higher than that in the circumferential direction for 10% and 12% gelMA grafts. Similar behavior was observed in the human internal mammary artery [62]. In addition, the anisotropic index values for all the printed gelMA grafts were found within the range of 0.60 to 2.00, as the reported index range for the human aorta [63] indicating that this printing method reproduces the structure of the native tissue to some extent. Along with the tensile testing of the graft specimens, burst pressure testing was also performed. No leakage was observed during the burst pressure testing, which represented the potential of the vertical additive-lathe printing method for the fabrication of tubular constructs. However, the burst pressure of the printed gelMA constructs were found to be far less than that of the native blood vessels. Thus, reinforcement is required to achieve better mechanical properties. For future directions, a bi-layered graft could be printed by depositing smooth muscle cells in the inner layer and fibroblast cells in the outer layer, whereas endothelial cells could be seeded in the lumen of the grafts to form a tight endothelium [64]. The low DoF gelMA was used for printing tubular constructs, as it offers high cell proliferation and spreading [65]. Overall, the vertical additive-lathe printing system could address the need for vascular grafts for the treatment of cardiovascular diseases.

5 Conclusion

The current study demonstrates that tubular grafts can be printed using a vertical additive-lathe printing system. It is feasible to print long and good-quality grafts using gelMA hydrogels. The 12% gelMA grafts showed the highest values of circumferential strength and burst pressure. Moreover, the printed grafts showed similar anisotropic behaviour as observed in the native human arteries. These results show great potential and lay a strong foundation for the printing of vascular grafts.

Acknowledgements

F. F. acknowledges the Higher Education Commission (HEC), Pakistan for the awarded PhD scholarship. The authors would like to thank Fergus Dingwall, Paul Aitken, Scott Cummings, and Katalin Kis of The University of Edinburgh for their help and support.

References:

[1] Organization WHC diseases (CVDs). Cardiovascular diseases (CVDs) 2017.

https://www.who.int/en/news-room/fact-sheets/detail/cardiovascular-diseases-(cvds) (accessed September 15, 2022).

[2] Amini M, Zayeri F, Salehi M. Trend analysis of cardiovascular disease mortality, incidence, and mortality-to-incidence ratio: results from global burden of disease study 2017. BMC Public Health 2021:1–12. https://doi.org/10.1186/s12889-021-10429-0.

[3] Leong DP, Joseph PG, McKee M, Anand SS, Teo KK, Schwalm JD, et al. Reducing the global burden of cardiovascular disease, part 2: Prevention and treatment of cardiovascular disease. Circ Res 2017;121:695–710. https://doi.org/10.1161/CIRCRESAHA.117.311849.

[4] Datta P, Ayan B, Ozbolat IT. Bioprinting for vascular and vascularized tissue biofabrication. Acta Biomater 2017;51:1–20. https://doi.org/10.1016/j.actbio.2017.01.035.

[5] Klinkert P, Post PN, Breslau PJ, Bockel JH Van. Saphenous Vein Versus PTFE for Above-Knee Femoropopliteal Bypass . A Review of the Literature. Eur J Vasc Endovasc Surg 2004;27:357–62. https://doi.org/10.1016/j.ejvs.2003.12.027.

[6] Ralf E. Harskamp, Renato D. Lopes, Clinton E. Baisden, Robbert J. de Winter JHA. Saphenous Vein Graft Failure After Coronary Artery Bypass Surgery. Ann Surg 2013;257:824–33. https://doi.org/10.1097/SLA.0b013e318288c38d.

[7] Maina RM, Barahona MJ, Finotti M, Lysyy T, Geibel P, Amico D, et al. Generating vascular conduits: from tissue engineering to three-dimensional bioprinting Scaffolds for TEVGs. Innov Surg Sci 2018;3:203–13. https://doi.org/10.1515/iss-2018-0016.

[8] Ong CS, Zhou X, Huang CY, Fukunishi T, Zhang H, Hibino N. Tissue engineered vascular grafts: current state of the field. Expert Rev Med Devices 2017;14:383–92. https://doi.org/10.1080/17434440.2017.1324293.

[9] Catto V, Farè S, Freddi G, Tanzi MC. Vascular Tissue Engineering: Recent Advances in Small Diameter Blood Vessel Regeneration. Hindawi 2014;2014:1–28. https://doi.org/https://doi.org/10.1155/2014/923030.

[10] Vliet JA Van Der, Kuppevelt TH Van. Vascular replacement using a layered elastin-collagen vascular graft in a porcine model: one week patency versus one month occlusion Vascular replacement using a layered elastin-collagen vascular graft in a porcine model : one week patency versus one mon. Organogenesis 2015;6278:105–21. https://doi.org/10.1080/15476278.2015.1038448.

[11] Koens MJW, Faraj KA, Wismans RG, Vliet JA Van Der, Krasznai AG, Cuijpers VMJI, et al. Controlled fabrication of triple layered and molecularly defined collagen/elastin vascular grafts resembling the native blood vessel. Acta Biomater 2010;6:4666–74. https://doi.org/10.1016/j.actbio.2010.06.038.

[12] Kumar VA, Caves JM, Haller CA, Dai E, Li L, Grainger S, et al. Acellular Vascular Grafts Generated from Collagen and Elastin Analogues. Acta Biomater 2014;9:8067–74. https://doi.org/10.1016/j.actbio.2013.05.024.Acellular.

[13] Awad NK, Niu H, Ali U. Electrospun Fibrous Scaffolds for Small-Diameter Blood Vessels : A Review. Membranes (Basel) 2018;8:1–26. https://doi.org/10.3390/membranes8010015.

[14] Ong CS, Nelson K, Ferris E, Geist GE, Youngblood B. Bilateral Arteriovenous Shunts as a Method for Evaluating Tissue-Engineered Vascular. Tissue Eng Part C 2017;23:728–35. https://doi.org/10.1089/ten.tec.2017.0217.

[15] Dobos A, Sai T, Grandhi P. Parallel fabrication of macroporous scaffolds. Biotechnol Bioeng

2018;115:1729–42. https://doi.org/10.1002/bit.26593.

[16] Xiong Y, Chan WY, Chua AWC, Feng J, Gopal P, Ong YS, et al. Decellularized Porcine Saphenous Artery for Small-Diameter Tissue-Engineered Conduit Graft. Artif Organs 2013;37:E74–E87. https://doi.org/10.1111/aor.12014.

[17] Lin C, Hsia K, Ma H, Lee H, Lu J. In Vivo Performance of Decellularized Vascular Grafts: A Review Article. Int J Mol Sci 2018;19:1–27. https://doi.org/10.3390/ijms19072101.

[18] Rayatpisheh S, Heath DE, Shakouri A, Rujitanaroj P, Yian S, Chan-park MB. Combining cell sheet technology and electrospun scaffolding for engineered tubular , aligned , and contractile blood vessels. Biomaterials 2014;35:2713–9. https://doi.org/10.1016/j.biomaterials.2013.12.035.

[19] Ahn H, Min Y, Takahashi H, Williams DF, Yoo JJ, Jin S, et al. Engineered small diameter vascular grafts by combining cell sheet engineering and electrospinning technology. Acta Biomater 2015;16:14–22. https://doi.org/10.1016/j.actbio.2015.01.030.

[20] Freeman S, Ramos R, Alexis P, Zhou L, Reeser K, Jin S, et al. A bioink blend for rotary 3D bioprinting tissue engineered small-diameter vascular constructs. Acta Biomater 2019;95:152–64. https://doi.org/10.1016/j.actbio.2019.06.052.

[21] Carrabba M, Madeddu P. Current Strategies for the Manufacture of Small Size Tissue Engineering Vascular Grafts. Front Bioeng Biotechnol 2018;6:1–12. https://doi.org/10.3389/fbioe.2018.00041.

[22] Song HG, Rumma RT, Ozaki CK, Edelman ER, Chen CS. Vascular Tissue Engineering: Progress, Challenges, and Clinical Promise. Stem Cell 2018;22:340–54. https://doi.org/10.1016/j.stem.2018.02.009.

[23] Mota C, Camarero-Espinosa S, Baker MB, Wieringa P, Moroni L. Bioprinting: From Tissue and Organ Development to in Vitro Models. Chem Rev 2020. https://doi.org/10.1021/acs.chemrev.9b00789.

[24] Hinton TJ, Jallerat Q, Palchesko RN, Park JH, Grodzicki MS, Shue HJ, et al. Three-dimensional printing of complex biological structures by freeform reversible embedding of suspended hydrogels. Sci Adv 2015;1. https://doi.org/10.1126/sciadv.1500758.

[25] Noor N, Shapira A, Edri R, Gal I, Wertheim L, Dvir T. 3D Printing of Personalized Thick and Perfusable Cardiac Patches and Hearts. Adv Sci 2019;6. https://doi.org/10.1002/advs.201900344.

[26] Krishnamoorthy S, Zhang Z, Xu C. Biofabrication of three-dimensional cellular structures based on gelatin methacrylate–alginate interpenetrating network hydrogel. J Biomater Appl 2019;33:1105–17. https://doi.org/10.1177/0885328218823329.

[27] Attalla R, Ling C, Selvaganapathy P. Fabrication and characterization of gels with integrated channels using 3D printing with microfluidic nozzle for tissue engineering applications. Biomed Microdevices 2016;18:1–12. https://doi.org/10.1007/s10544-016-0042-6.

[28] Giuseppe M Di, Law N, Webb B, A. Macrae R, Liew LJ, Sercombe TB, et al. Mechanical behaviour of alginate-gelatin hydrogels for 3D bioprinting. J Mech Behav Biomed Mater 2018;79:150–7. https://doi.org/10.1016/j.jmbbm.2017.12.018.

[29] Kesari P, Xu T, Boland T. Layer-by-layer printing of cells and its application to tissue engineering. MRS Proc 2005;845:AA4.5. https://doi.org/10.1557/PROC-845-AA4.5.

[30] Nakamura M, Nishiyama Y, Henmi C, Iwanaga S, Nakagawa H, Yamaguchi K, et al. Ink jet

three-dimensional digital fabrication for biological tissue manufacturing: Analysis of alginate microgel beads produced by ink jet droplets for three dimensional tissue fabrication. J Imaging Sci Technol 2008;52:0602011–6. https://doi.org/10.2352/J.ImagingSci.Technol.(2008)52:6(060201).

[31] Christensen K, Xu C, Chai W, Zhang Z, Fu J. Freeform Inkjet Printing of Cellular Structures with Bifurcations. Biotechnol Bioeng 2015;112:1047–55. https://doi.org/10.1002/bit.25501.

[32] Xu C, Chai W, Huang Y, Markwald RR. Scaffold-free inkjet printing of three-dimensional zigzag cellular tubes. Biotechnol Bioeng 2012;109:3152–60. https://doi.org/10.1002/bit.24591.

[33] Ji Y, Yang Q, Huang G, Shen M, Jian Z, Thoraval MJ, et al. Improved Resolution and Fidelity of Droplet-Based Bioprinting by Upward Ejection. ACS Biomater Sci Eng 2019;5:4112–21. https://doi.org/10.1021/acsbiomaterials.9b00400.

[34] Wu PK, Ringeisen BR. Development of human umbilical vein endothelial cell (HUVEC) and human umbilical vein smooth muscle cell (HUVSMC) branch/stem structures on hydrogel layers via biological laser printing (BioLP). Biofabrication 2010;2. https://doi.org/10.1088/1758-5082/2/1/014111.

[35] Xiong R, Zhang Z, Chai W, Huang Y, Chrisey DB. Freeform drop-on-demand laser printing of 3D alginate and cellular constructs. Biofabrication 2015;7. https://doi.org/10.1088/1758-5090/7/4/045011.

[36] Laura Elomaa, Chi-Chun Pan, Yaser Shanjani, Andrey Malkovskiy, Jukka V. Seppälä YY. Three-dimensional fabrication of cell-laden biodegradable poly(ethylene glycol-co-depsipeptide) hydrogels by visible light stereolithography Laura. J Mater Chem B Mater Biol Med 2015;42:8348–58. https://doi.org/10.1016/j.physbeh.2017.03.040.

[37] Wadnap S, Krishnamoorthy S, Zhang Z, Xu C. Biofabrication of 3D cell-encapsulated tubular constructs using dynamic optical projection stereolithography. J Mater Sci Mater Med 2019;30. https://doi.org/10.1007/s10856-019-6239-5.

[38] Krishnamoorthy S, Wadnap S, Noorani B, Xu H, Xu C. Investigation of gelatin methacrylate working curves in dynamic optical projection stereolithography of vascular-like constructs. Eur Polym J 2020;124:109487. https://doi.org/10.1016/j.eurpolymj.2020.109487.

[39] Fazal F, Raghav S, Callanan A, Koutsos V, Radacsi N. Recent advancements in the bioprinting of vascular grafts. Biofabrication 2021;13. https://doi.org/10.1088/1758-5090/ac0963.

[40] Gillispie G, Prim P, Copus J, Fisher J, Mikos AG, Yoo JJ, et al. Assessment methodologies for extrusion-based bioink printability. Biofabrication 2020;12:1–28. https://doi.org/10.1088/1758-5090/ab6f0d.

[41] Gao G, Kim BS, Jang J, Cho DW. Recent Strategies in Extrusion-Based Three-Dimensional Cell Printing toward Organ Biofabrication. ACS Biomater Sci Eng 2019;5:1150–69. https://doi.org/10.1021/acsbiomaterials.8b00691.

[42] Sundaramurthi D, Rauf S, Hauser CAE. 3D bioprinting technology for regenerative medicine applications. Int J Bioprinting 2016;2:9–26. https://doi.org/10.18063/IJB.2016.02.010.

[43] Jiang T, Munguia-Lopez JG, Flores-Torres S, Kort-Mascort J, Kinsella JM. Extrusion bioprinting of soft materials: An emerging technique for biological model fabrication. Appl Phys Rev 2019;6. https://doi.org/10.1063/1.5059393.

[44] Müller M, Becher J. Bioink properties before, during, and after 3D bioprinting. Biofabrication 2016;8:1–19.

[45] Ozbolat IT, Hospodiuk M. Current advances and future perspectives in extrusion-based bioprinting. Biomaterials 2016;76:321–43. https://doi.org/10.1016/j.biomaterials.2015.10.076.

[46] Holland I, Logan J, Shi J, Mccormick C, Liu D, Shu W. 3D biofabrication for tubular tissue engineering. Bio-Design Manuf 2018;1:89–100. https://doi.org/10.1007/s42242-018-0013-2.

[47] Zhuang P, Ng WL, An J, Chua CK, Tan LP. Layer-by-layer ultraviolet assisted extrusion-based (UAE) bioprinting of hydrogel constructs with high aspect ratio for soft tissue engineering applications. PLoS One 2019;14:1–21. https://doi.org/10.1371/journal.pone.0216776.

[48] Xu L, Varkey M, Jorgensen A, Ju J hui, Jin Q, Park JH, et al. Bioprinting small diameter blood vessel constructs with an endothelial and smooth muscle cell bilayer in a single step. Biofabrication 2020;12:1–14. https://doi.org/10.1088/1758-5090/aba2b6.

[49] Liu H, Zhou H, Chairinnas. The synchronization among nozzle extrusion, nozzle speed and rotating speed based on 3D vessel bioprinter. Proc 2016 Int Conf Instrumentation, Control Autom ICA 2016 2017:160–5. https://doi.org/10.1109/ICA.2016.7811494.

[50] Reeser K, Doiron AL. Three-Dimensional Printing on a Rotating Cylindrical Mandrel: A Review of Additive-Lathe 3D Printing Technology. 3D Print Addit Manuf 2019;6:293–307. https://doi.org/10.1089/3dp.2019.0058.

[51] Liu J, Zhang B, Li L, Yin J, Fu J. Bioactive Materials Additive-lathe 3D bioprinting of bilayered nerve conduits incorporated with supportive cells. Bioact Mater 2021;6:219–29. https://doi.org/10.1016/j.bioactmat.2020.08.010.

[52] Liu H, Zhou H, Lan H, Liu T, Liu X, Yu H. 3D printing of artificial blood vessel: study on multi-parameter optimization design for vascular molding effect in alginate and gelatin. Micromachines 2017;8:1–10. https://doi.org/10.3390/mi8080237.

[53] Li L, Qin S, Peng J, Chen A, Nie Y, Liu T, et al. Engineering gelatin-based alginate/carbon nanotubes blend bioink for direct 3D printing of vessel constructs. Int J Biol Macromol 2020;145:262–71. https://doi.org/10.1016/j.ijbiomac.2019.12.174.

[54] Ying G, Jiang N, Yu C, Zhang YS. Three-dimensional bioprinting of gelatin methacryloyl (GelMA). Bio-Design Manuf 2018;1:215–24. https://doi.org/10.1007/s42242-018-0028-8.

[55] Bulcke AI Van Den, Bogdanov B, Rooze N De, Schacht EH, Cornelissen M, Berghmans H. Structural and rheological properties of methacrylamide modified gelatin hydrogels. Biomacromolecules 2000;1:31–8. https://doi.org/10.1021/bm990017d.

[56] Fazal F, Javier F, Sanchez D, Waqas M, Koutsos V, Callanan A, et al. A modified 3D printer as a hybrid bioprinting-electrospinning system for use in vascular tissue engineering applications. Med Eng Phys 2021;94:52–60. https://doi.org/10.1016/j.medengphy.2021.06.005.

[57] Laterreur V, Ruel J, Auger FA, Vallières K, Tremblay C, Lacroix D, et al. Comparison of the direct burst pressure and the ring tensile test methods for mechanical characterization of tissue-engineered vascular substitutes. J Mech Behav Biomed Mater 2014;34:253–63. https://doi.org/10.1016/j.jmbbm.2014.02.017.

[58] Melchels FPW, Fehr I, Reitz AS, Dunker U, Beagley KW, Dargaville TR, et al. Initial design and physical characterization of a polymeric device for osmosis-driven delayed burst delivery of vaccines. Biotechnol Bioeng 2015;112:1927–35. https://doi.org/10.1002/bit.25593.

[59] Laronda MM, Rutz AL, Xiao S, Whelan KA, Duncan FE, Roth EW, et al. A bioprosthetic ovary created using 3D printed microporous scaffolds restores ovarian function in sterilized mice.

Nat Commun 2017;8:1–10. https://doi.org/10.1038/ncomms15261.

[60] Sánchez EM, Gómez-blanco JC, Nieto EL, Casado JG, Macías-garcía A, Díez MAD, et al. Hydrogels for Bioprinting: A Systematic Review of Hydrogels Synthesis, Bioprinting Parameters, and Bioprinted Structures Behavior Bioprinting Pre-printing. Front Bioeng Biotechnol 2020;8. https://doi.org/10.3389/fbioe.2020.00776.

[61] Melchels FPW, Dhert WJA, Hutmacher DW, Malda J. Development and characterisation of a new bioink for additive tissue manufacturing. J Mater Chem B 2014;2:2282–9. https://doi.org/10.1039/c3tb21280g.

[62] Camasão DB, Mantovani D. The mechanical characterization of blood vessels and their substitutes in the continuous quest for physiological-relevant performances. A critical review. Mater Today Bio 2021;10. https://doi.org/10.1016/j.mtbio.2021.100106.

[63] Okamoto RJ, Wagenseil JE, DeLong WR, Peterson SJ, Kouchoukos NT, Sundt TM. Mechanical properties of dilated human ascending aorta. Ann Biomed Eng 2002;30:624–35. https://doi.org/10.1114/1.1484220.

[64] Klotz BJ, Lim KS, Chang YX, Soliman BG, Pennings I, Melchels FPW, et al. Engineering of a complex bone tissue model with endothelialised channels and capillary-like networks. Eur Cells Mater 2018;35:335–49. https://doi.org/10.22203/eCM.v035a23.

[65] Pepelanova I, Kruppa K, Scheper T, Lavrentieva A. Gelatin-methacryloyl (GelMA) hydrogels with defined degree of functionalization as a versatile toolkit for 3D cell culture and extrusion bioprinting. Bioengineering 2018;5. https://doi.org/10.3390/bioengineering5030055.